Supplementary Material for: Improved Estimation of Bird Abundance and Energy Consumption by Combining Point and Transect Observations

Maria Jose Ayala Bolagay, Aaron Brothers, Marta Quitián, Eike Lena Neuschulz, Matthias Schleuning, Katrin Böhning-Gaese, Orlando Alvarez, Vinicio Santillán, Christopher Thron

Supplement A: Model fit diagnostics

This supplement contains scatter plots of actual versus predicted transect observations for the two-coefficient model (Figures A1–A4) and the one-coefficient model (Figures A5–A8), organized by location, elevation, habitat type, and combined.

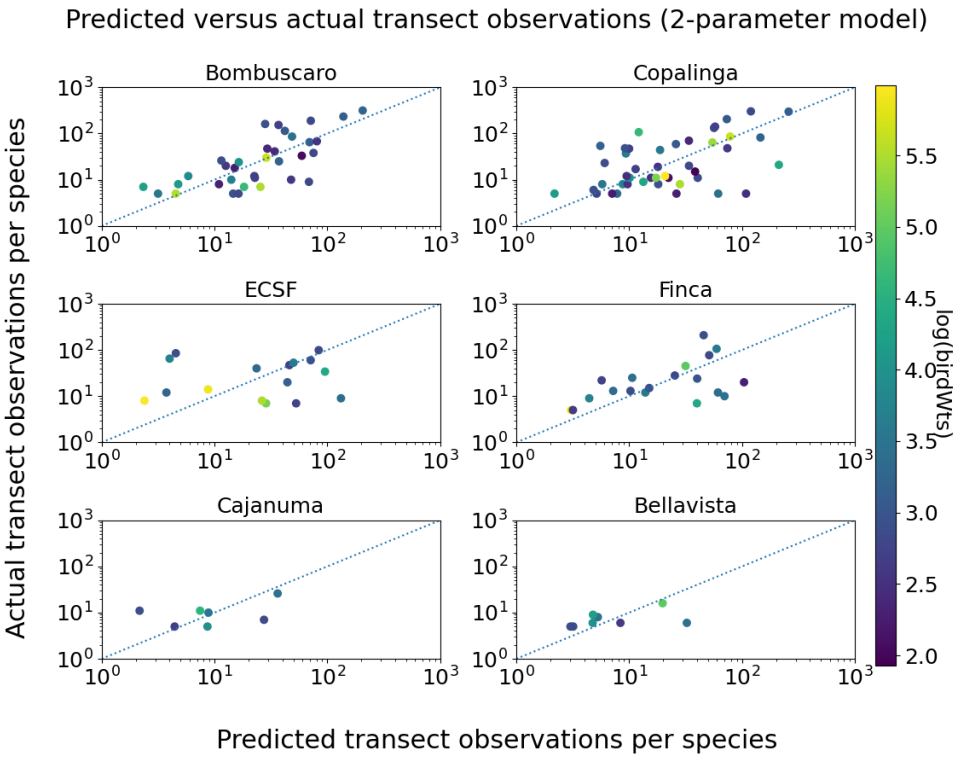


Fig. A1 Transect observation prediction accuracy by location for the two-coefficient model (13) that includes both bird weight and fruit weight as predictors. Each panel shows log-scale actual versus log-scale predicted transect observations for one of the six study sites, with point color indicating mean bird species weight. The 45-degree line corresponds to zero prediction error. Scatter around the line reflects residual variability not explained by bird weight or fruit weight.

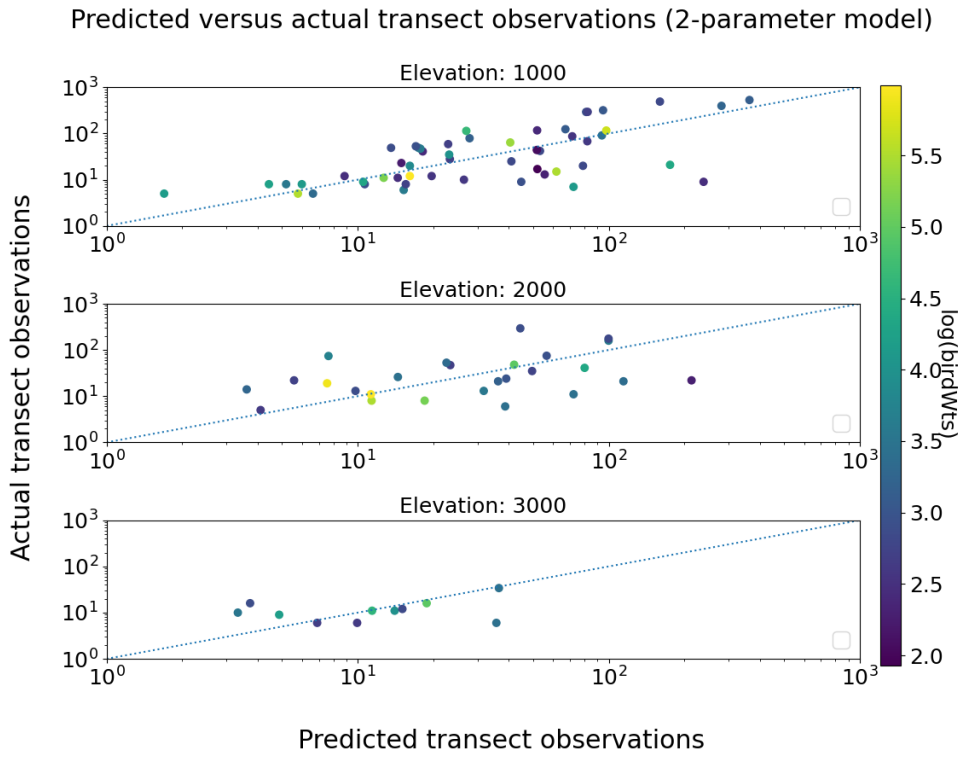


Fig. A2 Transect observation prediction accuracy of the two-coefficient model (13) (bird weight + fruit weight), with species data pooled by elevation. Low (1000 m), mid (2000 m), and high (3000 m) elevation panels each combine data from the two sites at that elevation. Axes and line as in Figure A1.

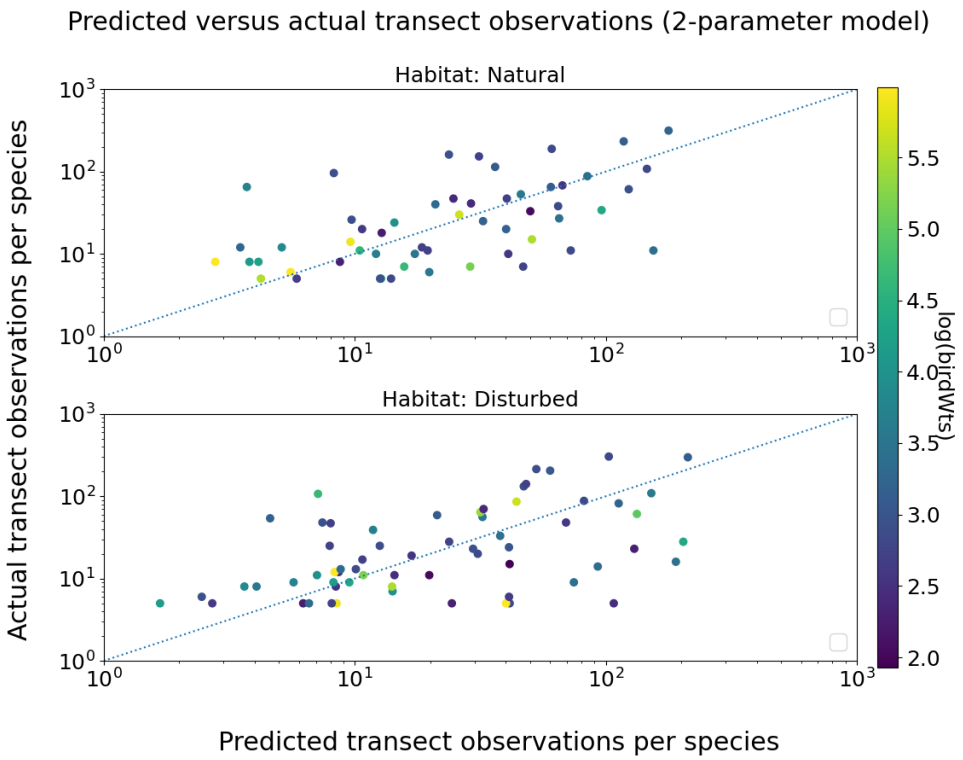


Fig. A3 Transect observation prediction accuracy of the two-coefficient model (13) (bird weight + fruit weight), with species data pooled by habitat type. Natural forest and fragmented forest panels each combine data from the three sites of that habitat type. Axes and line as in Figure A1.

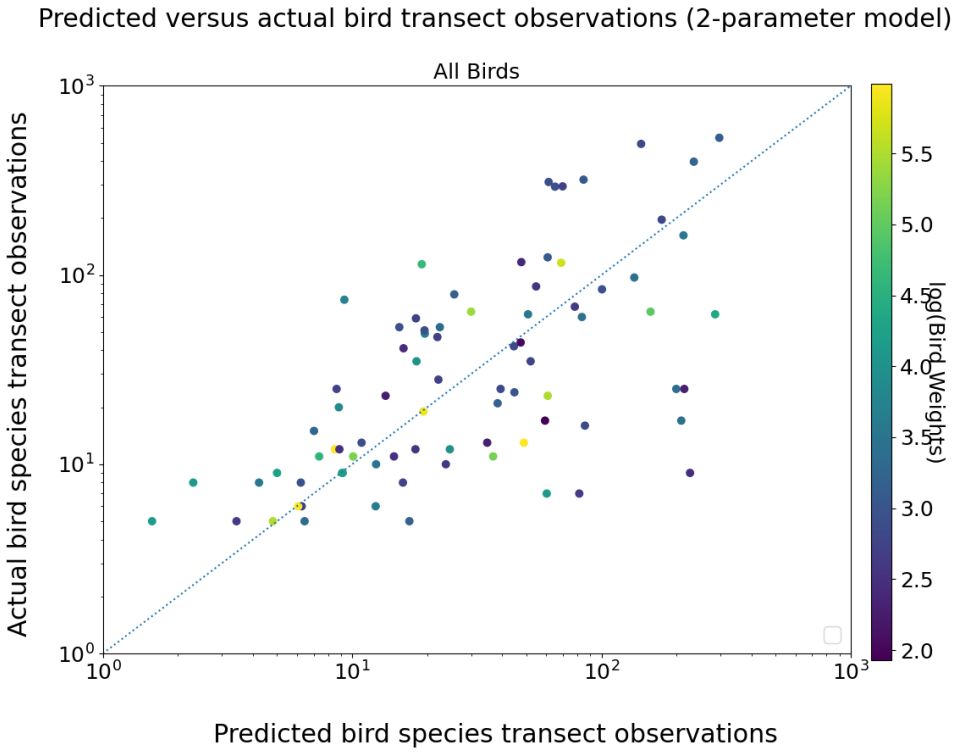


Fig. A4 Transect observation prediction accuracy for the two-coefficient model (13) (bird weight + fruit weight) using all species observations from all six sites combined. Axes and line as in Figure A1.

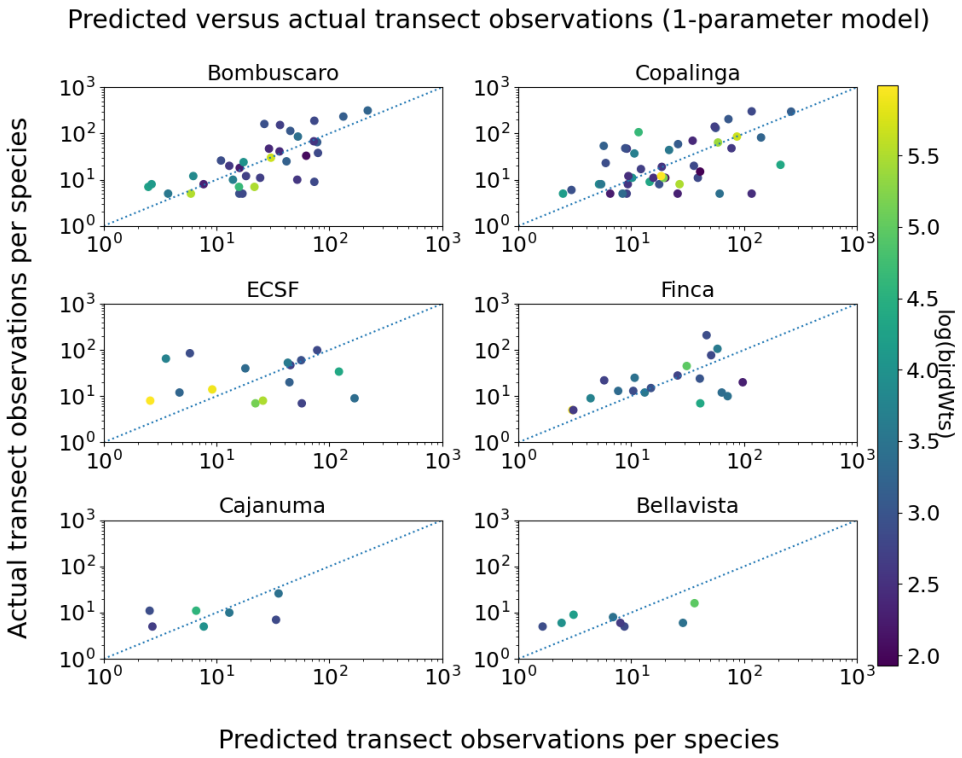


Fig. A5 Transect observation prediction accuracy by location for the one-coefficient model (47), which includes bird weight only ($p_f = 0$). Compare with Figure A1 for the two-coefficient model. Axes and line as in Figure A1.

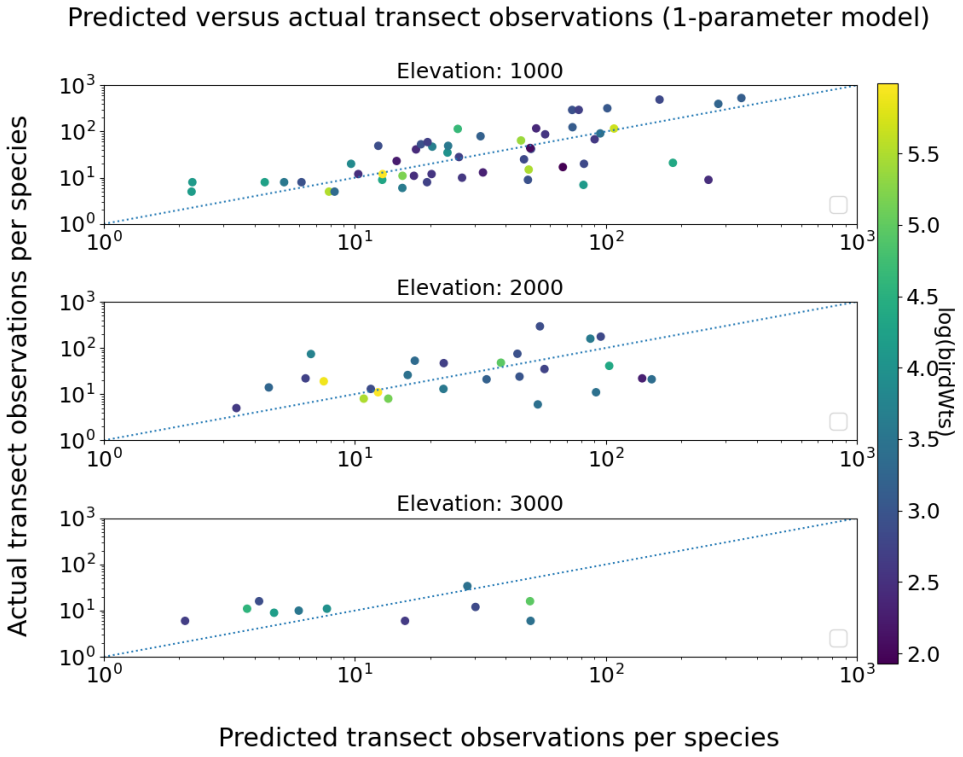


Fig. A6 Transect observation prediction accuracy for the one-coefficient model (47) (bird weight only), with species data pooled by elevation. Compare with Figure A2. Axes and line as in Figure A1.

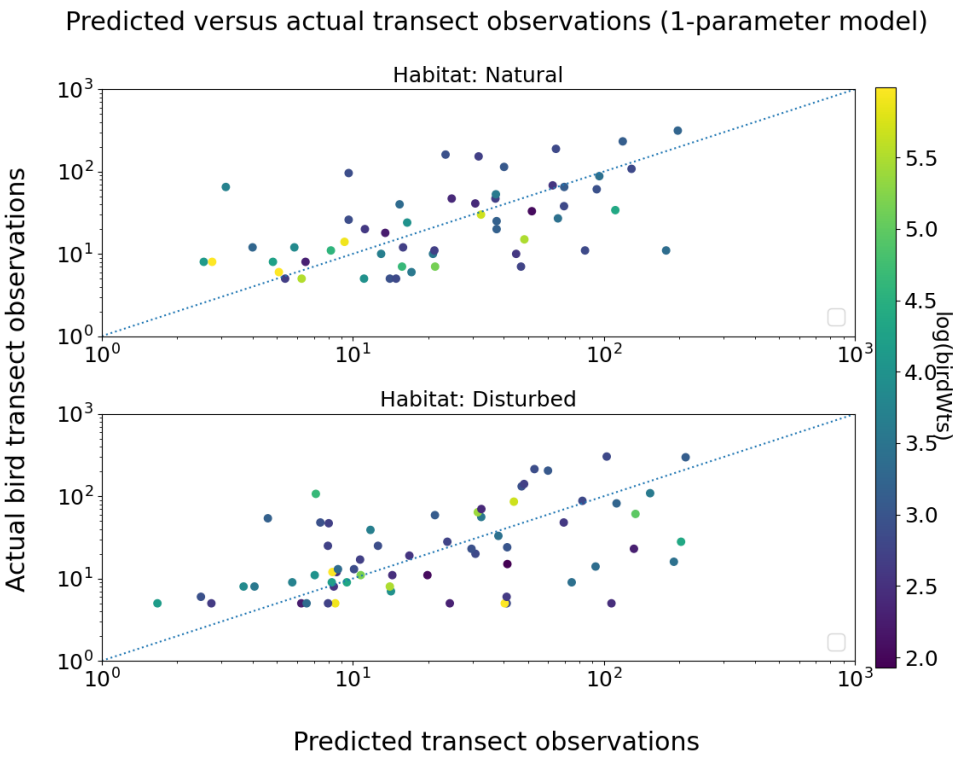


Fig. A7 Transect observation prediction accuracy for the one-coefficient model (47) (bird weight only), with species data pooled by habitat type. Compare with Figure A3. Axes and line as in Figure A1.

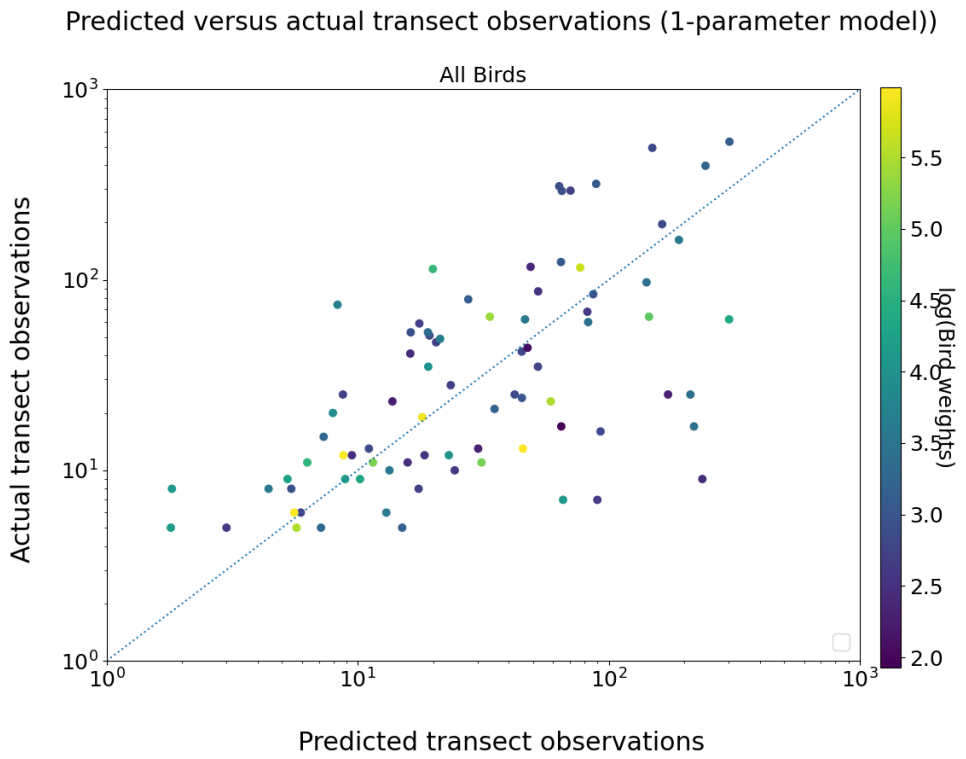


Fig. A8 Transect observation prediction accuracy for the one-coefficient model (47) (bird weight only), using all species observations from all six sites combined. Compare with Figure A4. Axes and line as in Figure A1.

Supplement B: Estimator bias, variance, and RMSE using mean bird weight exponent $\bar{p}_b$ (case a)

This supplement contains detailed performance evaluation figures for the point count-based, transect-based, and combined estimators of relative abundance and log relative abundance, computed using the mean value $\bar{p}_b$ of the bird weight exponent (case a as defined in Section 3.2.3).

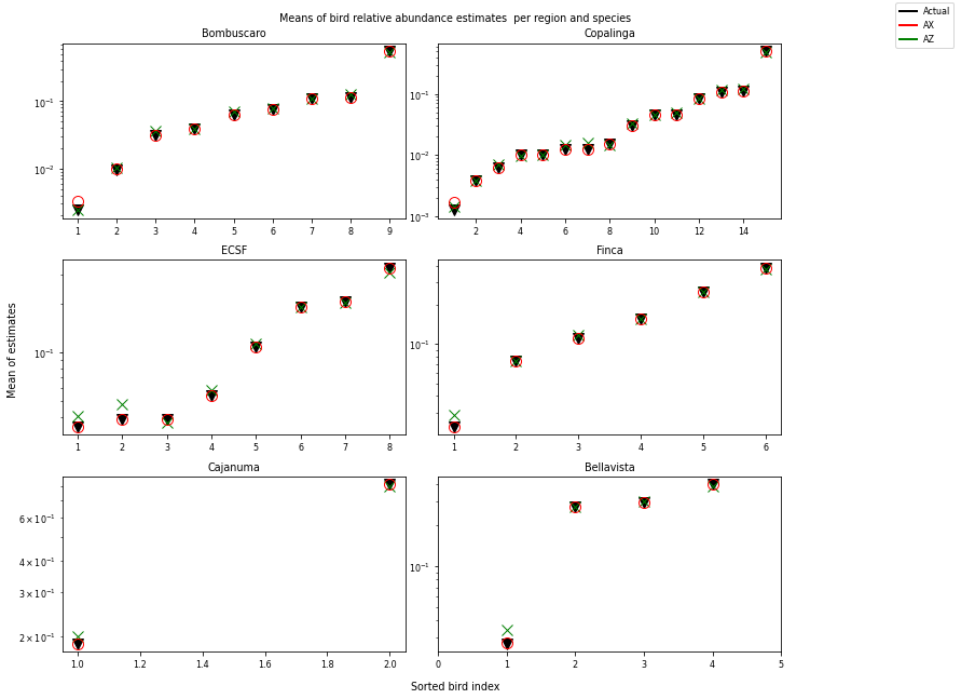


Fig. B1 Mean values of the point count-based estimator $(\widehat{a}_n)_z$ (circles) and the transect-based estimator $(\widehat{a}_n)_x$ (triangles) over 10,000 simulations, compared to true relative abundance (dashed line), for bird families at each of the six study sites. The transect estimator is computed using the mean bird weight exponent $\bar{p}_b$ (case a). Within each site panel, families are sorted in order of increasing true relative abundance. Both estimators show little systematic bias, with slightly larger departures for rare families.

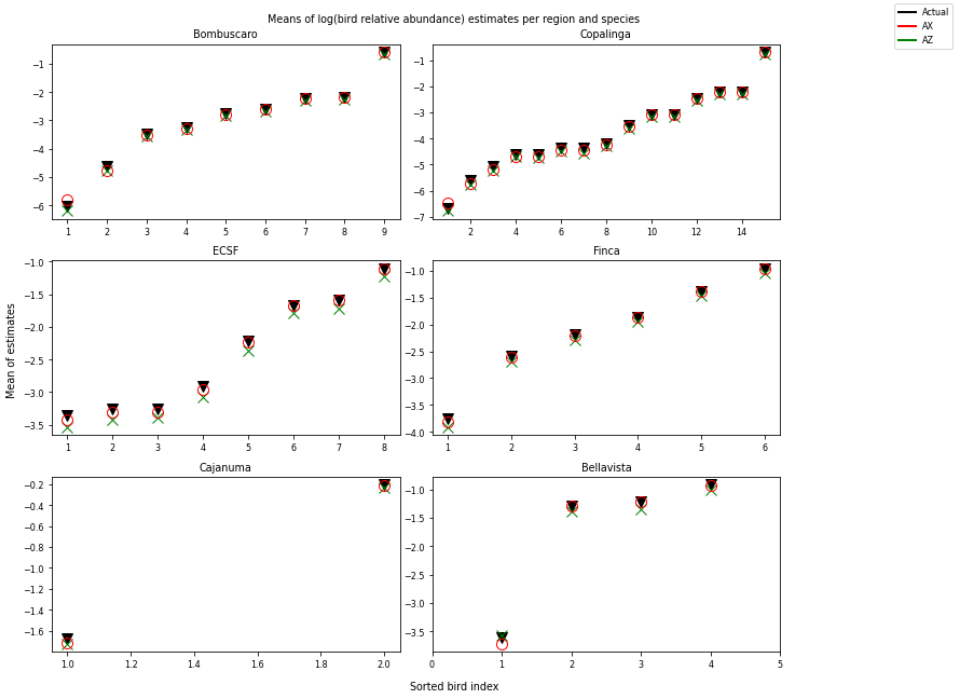


Fig. B2 Mean values of the point count-based log abundance estimator $(\widehat{\ell}_n)_z$ (circles) and the transect-based log abundance estimator $(\widehat{\ell}_n)_x$ (triangles) over 10,000 simulations, compared to true log relative abundance (dashed line), for bird families at each of the six study sites. The transect estimator uses the mean bird weight exponent $\bar{p}_b$ (case a). Families are sorted as in Figure B1.

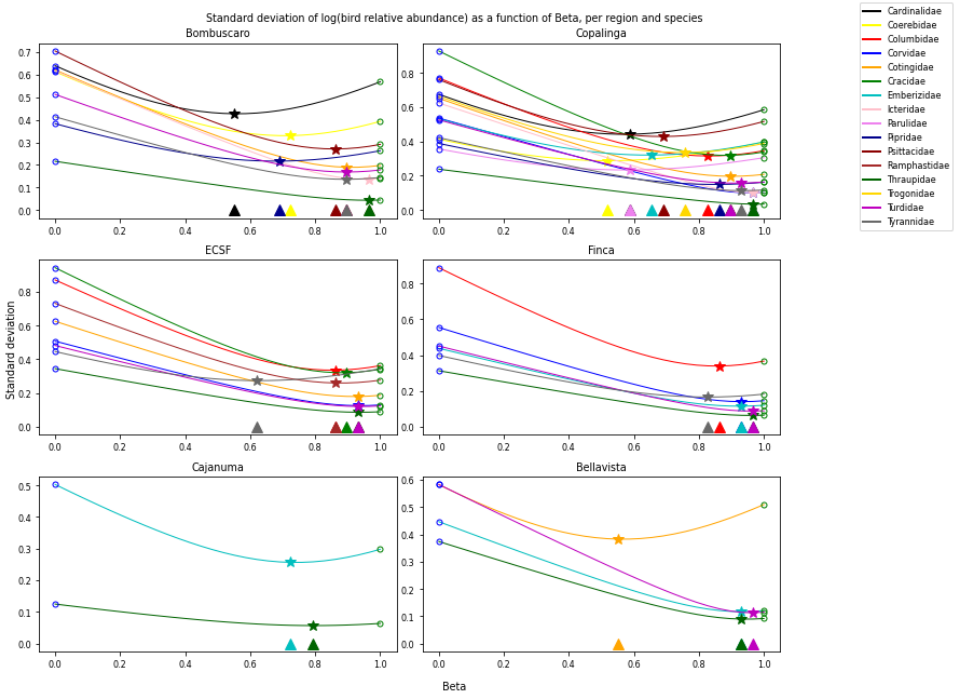


Fig. B3 Standard deviation of the combined log abundance estimator $(\widehat{\ell}_n)_\beta$ as a function of $\beta \in [0,1]$, for each bird family in each of the six study sites. $\beta = 0$ corresponds to $(\widehat{\ell}_n)_X$ (transect-based); $\beta = 1$ corresponds to $(\widehat{\ell}_n)_Z$ (point count-based). Stars mark the minimum of each curve; triangles on the x-axis indicate the theoretically optimal β from (35). Transect estimator uses $\bar{p}_b$ (case a).

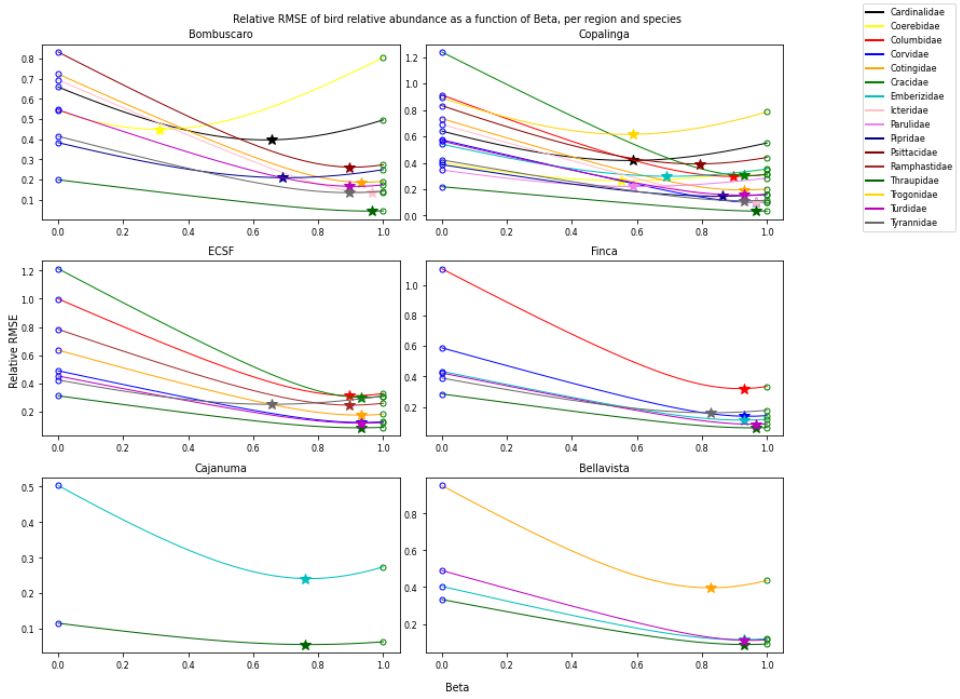


Fig. B4 Relative root mean squared error (RMSE divided by true relative abundance) of the combined estimator $(\widehat{a}_n)_\beta$ as a function of $\beta \in [0, 1]$, for each bird family in each site. $\beta = 0$ corresponds to $(\widehat{a}_n)_X$; $\beta = 1$ to $(\widehat{a}_n)_Z$. Stars and triangles as in Figure 4 of the main body. The near-identical appearance of this figure and Figure 4 confirms that bias is negligible relative to variance. Transect estimator uses $\bar{p}_b$ (case a).

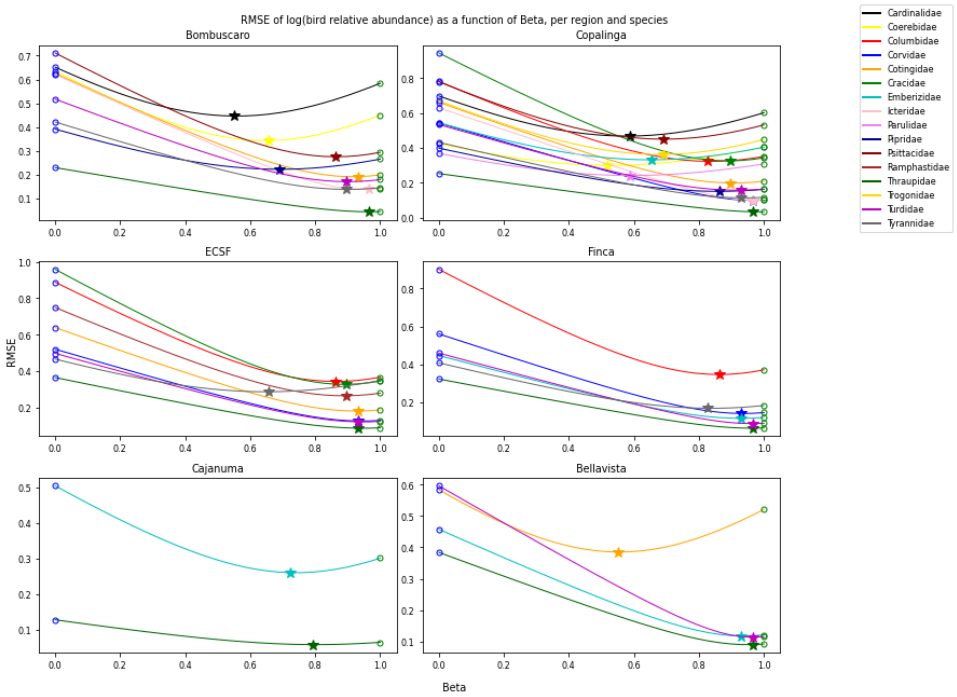


Fig. B5 Root mean squared error (RMSE) of the combined log abundance estimator $(\widehat{\ell_n})_\beta$ as a function of $\beta \in [0, 1]$, for each bird family in each site. $\beta = 0$ corresponds to $(\widehat{\ell_n})_X$; $\beta = 1$ to $(\widehat{\ell_n})_Z$. Stars and triangles as in Figure B3. Transect estimator uses $\bar{p}_b$ (case a).

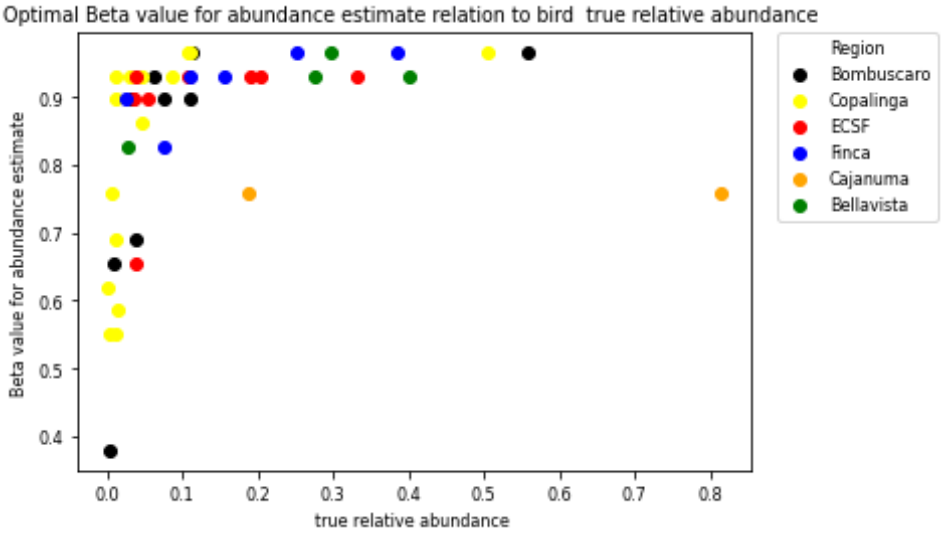


Fig. B6 RMSE-minimizing value of β for the combined relative abundance estimator $(\widehat{a}_n)_\beta$, plotted against the true relative abundance of each bird family, for all families across all six sites. Each point represents one family-site combination. Lower β values (giving more weight to the transect estimator) occur predominantly for rare families (true relative abundance below 0.1), while common families consistently receive high β (closer to the point count estimator). Transect estimator uses $\bar{p}_b$ (case a).

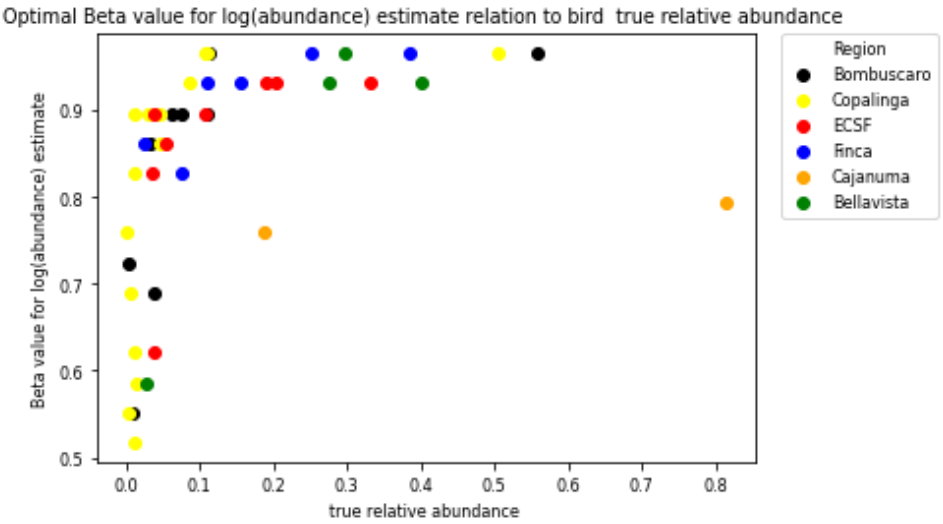


Fig. B7 RMSE-minimizing value of β for the combined log abundance estimator $(\widehat{\ell}_n)_\beta$, plotted against true relative abundance. Layout and interpretation as in Figure B6. Transect estimator uses $\bar{p}_b$ (case a).

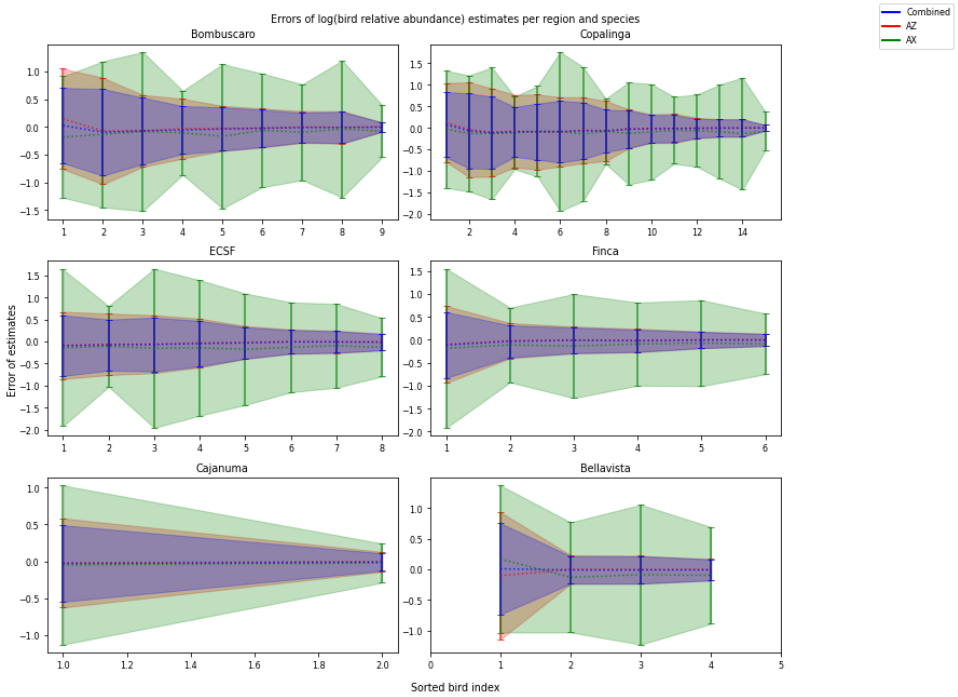


Fig. B8 95% confidence intervals for the error of three log abundance estimators: $(\widehat{\ell_n})_Z$ (labeled AZ), $(\widehat{\ell_n})_X$ (labeled AX), and the combined estimator $(\widehat{\ell_n})_\beta$. Results are shown for each bird family in each site. The AX and combined estimators use $\bar{p}_b$ (case a). Families are ordered by increasing true relative abundance within each site panel.

Supplement C: Estimator bias, variance, and RMSE using exact bird weight exponent $p_{b,n}$ (case b)

This supplement contains figures corresponding to those in Supplement B, but computed using the exact bird weight exponent $p_{b,n}$ for each family (case b as defined in Section 3.2.3). Comparison with Supplement B illustrates the improvement in estimator accuracy that results from precise knowledge of the weight-energy relationship.

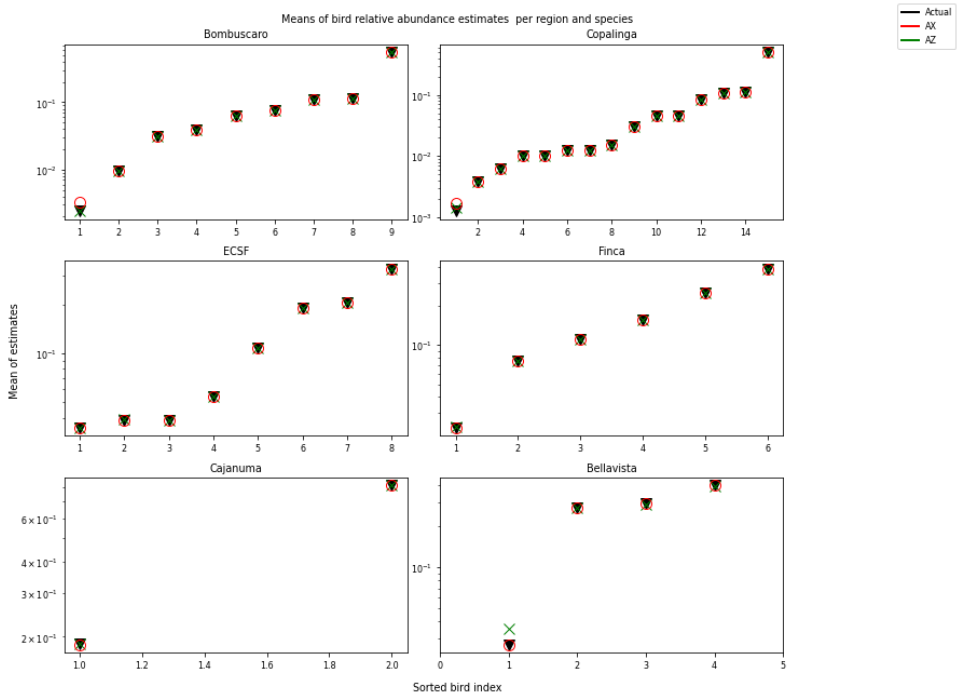


Fig. C1 As Supplement B Figure B1, but with the transect-based estimator computed using the exact bird weight exponent $p_{b,n}$ for each family (case b). Compared to Figure B1, the transect estimator shows reduced bias and tighter agreement with the true values, demonstrating the benefit of accurate knowledge of the weight-energy relationship.

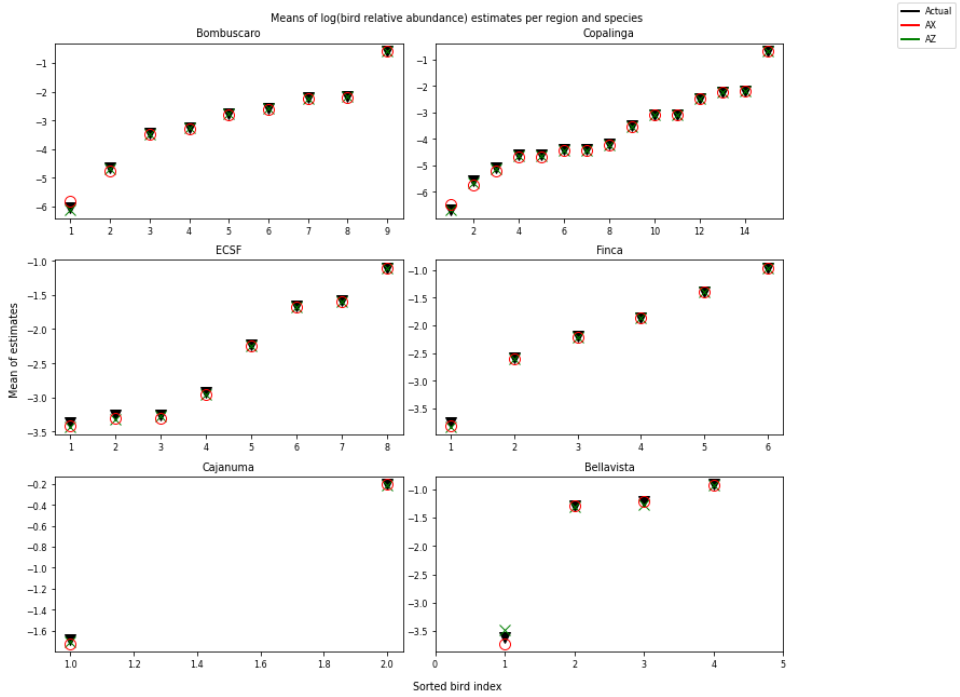


Fig. C2 As Supplement B Figure B2, but with the transect-based log abundance estimator computed using the exact bird weight exponent $p_{b,n}$ for each family (case b). Families are sorted as in Figure B1.

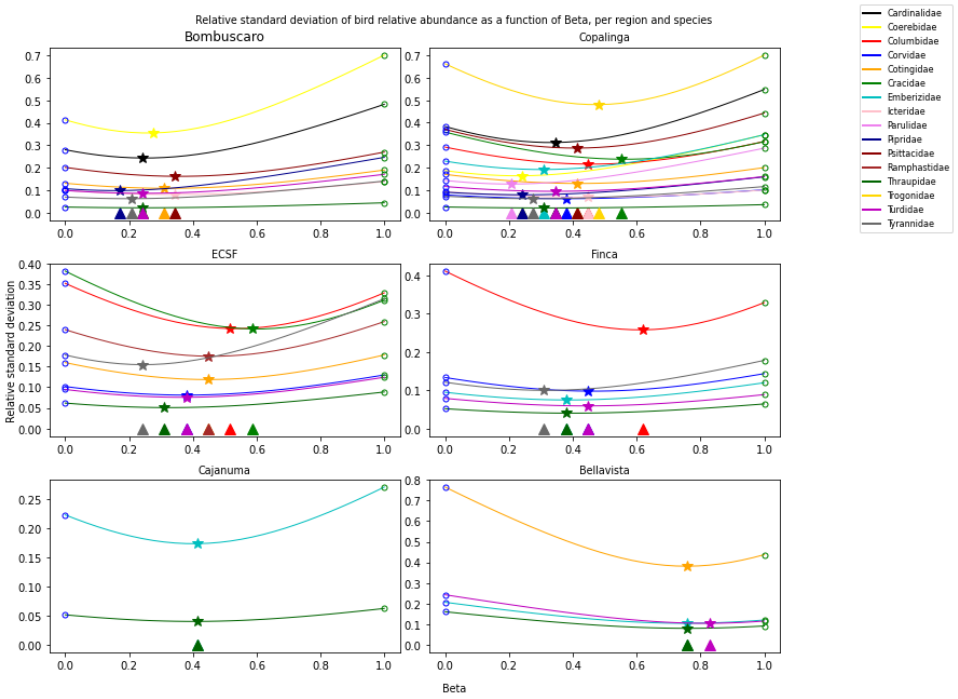


Fig. C3 As main body Figure 4, but with the transect estimator using the exact bird weight exponent $p_{b,n}$ (case b). The minimum standard deviation at $\beta = 0$ (pure transect estimator) is markedly lower than in Figure 4, and optimal β values shift toward lower values, reflecting the improved accuracy of the transect estimator when $p_{b,n}$ is known precisely.

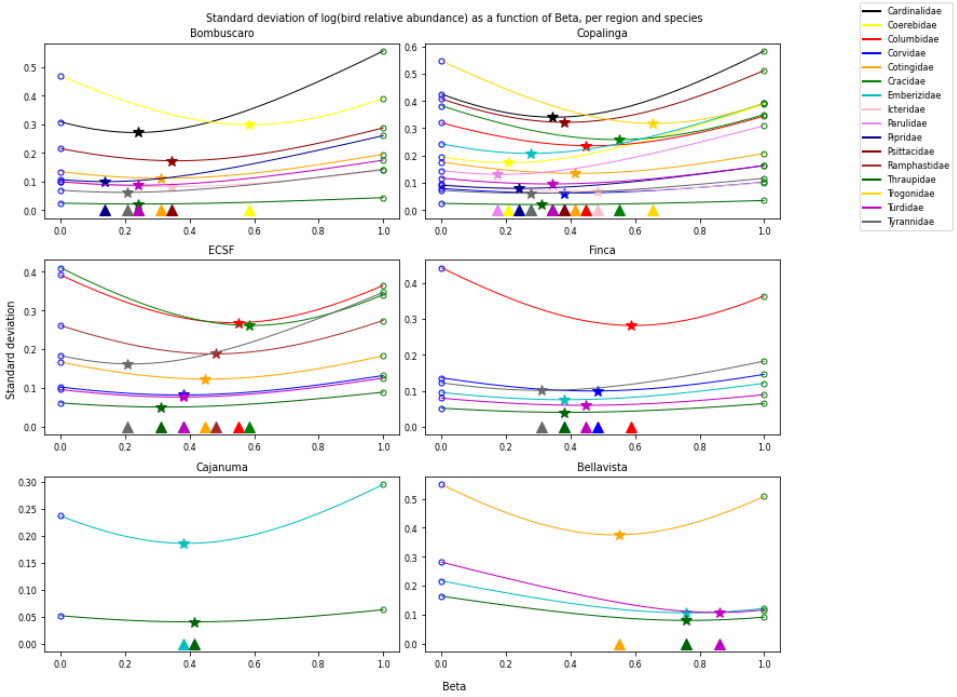


Fig. C4 As Supplement B Figure B3, but with the transect log abundance estimator using the exact bird weight exponent $p_{b,n}$ (case b). Optimal β values shift toward lower values compared to Figure B3, reflecting the improved transect estimator accuracy.

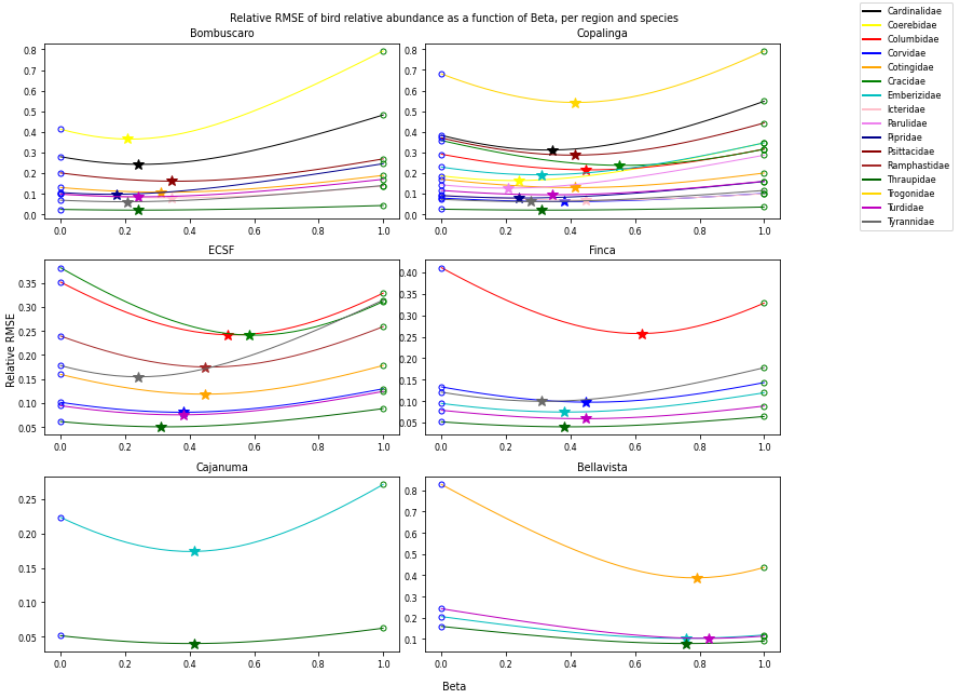


Fig. C5 As Supplement B Figure B4, but with the transect estimator using the exact bird weight exponent $p_{b,n}$ (case b). Minimum relative RMSE values are substantially lower than in Figure B4, confirming the advantage of precise knowledge of the weight-energy exponent.

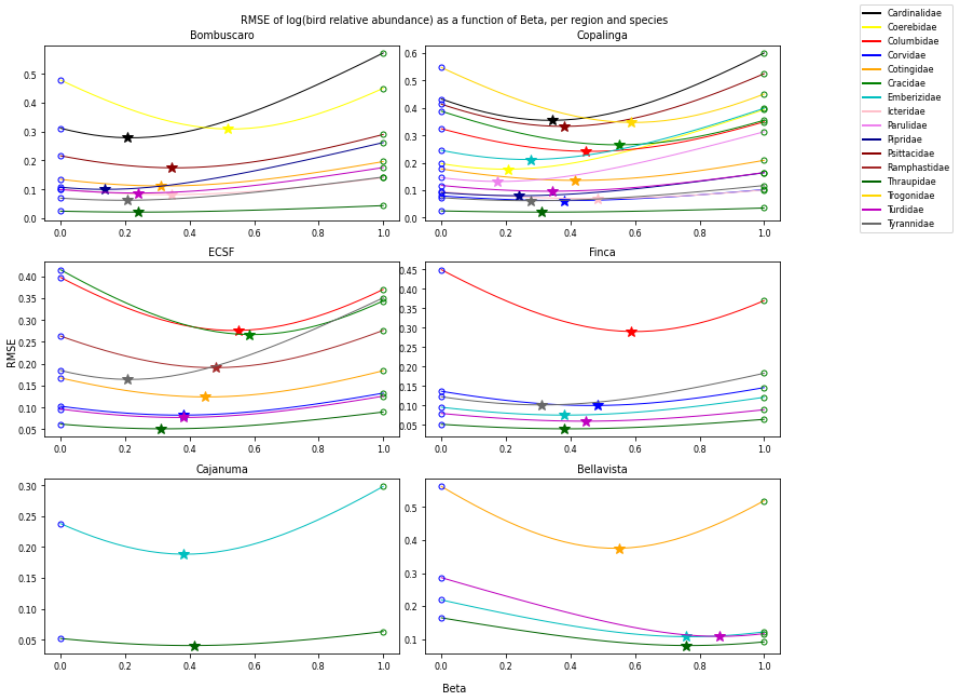


Fig. C6 As Supplement B Figure B5, but with the transect log abundance estimator using the exact bird weight exponent $p_{b,n}$ (case b). Minimum RMSE values are reduced relative to Figure B5.

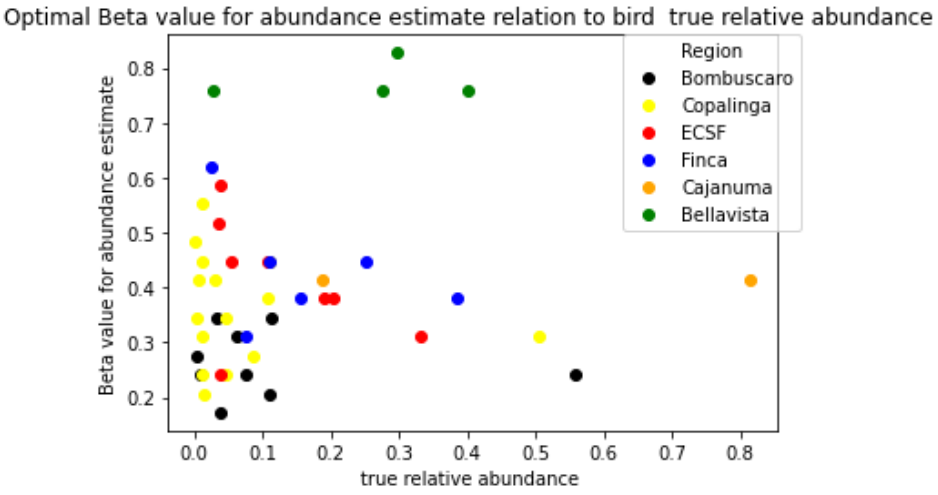


Fig. C7 As Supplement B Figure B6, but with the transect estimator using the exact bird weight exponent $p_{b,n}$ (case b). Optimal β values are generally lower than in Figure B6, indicating that more weight is appropriately assigned to the transect estimator when $p_{b,n}$ is known precisely.

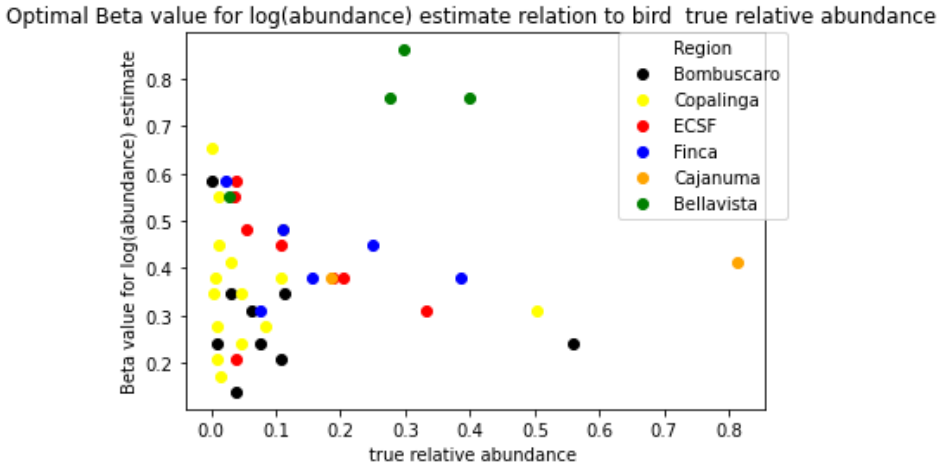


Fig. C8 As Supplement B Figure B7, but with the transect log abundance estimator using the exact bird weight exponent $p_{b,n}$ (case b). Layout and interpretation as in Figure C7.

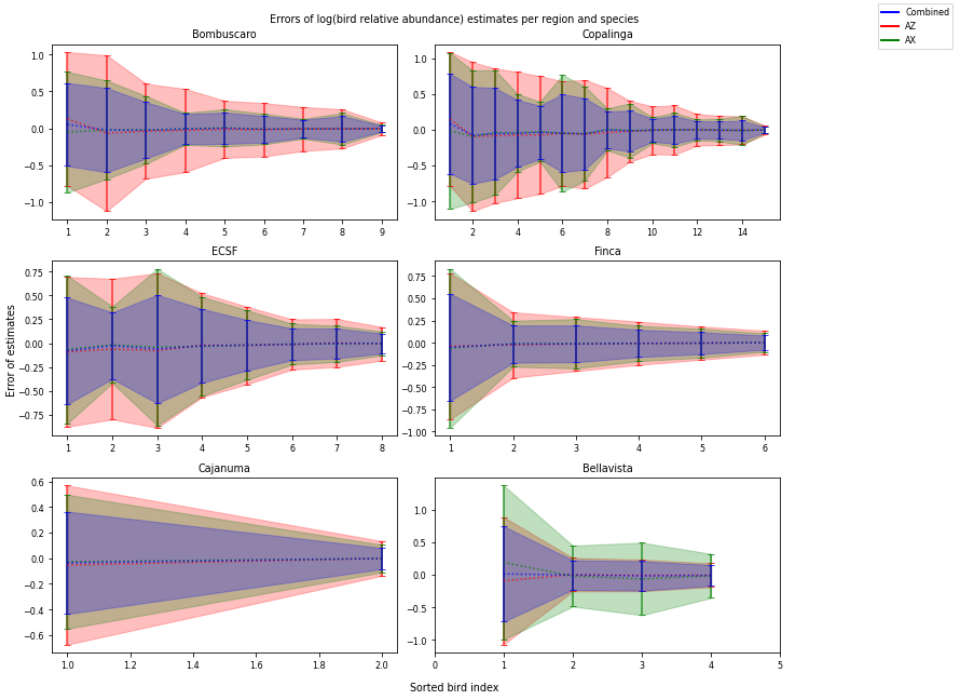


Fig. C9 As Supplement B Figure B8, but with the transect-based and combined log abundance estimators using the exact bird weight exponent $p_{b,n}$ (case b). Confidence intervals are substantially narrower for the transect and combined estimators compared to Figure B8.